Degradation of protein translation machinery by amino acid starvation-induced macroautophagy

Gretzmeier, Christine ; Eiselein, Sven ; Johnson, Gregory R ; Engelke, Rudolf ; Nowag, Heike ; Zarei, Mostafa ; Küttner, Victoria ; Becker, Andrea C ; Rigbolt, Kristoffer T G ; Høyer-Hansen, Maria ; Andersen, Jens S ; Münz, Christian ; Murphy, Robert F ; Dengjel, Jörn

Abstract: Macroautophagy is regarded as a nonspecific bulk degradation process of cytoplasmic material within the lysosome. However, the process has mainly been studied by nonspecific bulk degradation assays using radiolabeling. In the present study we monitor protein turnover and degradation by global, unbiased approaches relying on quantitative mass spectrometry-based proteomics. Macroautophagy is induced by rapamycin treatment, and by amino acid and glucose starvation in differentially, metabolically labeled cells. Protein dynamics are linked to image-based models of autophagosome turnover. Depending on the inducing stimulus, protein as well as organelle turnover differ. Amino acid starvation-induced macroautophagy leads to selective degradation of proteins important for protein translation. Thus, protein dynamics reflect cellular conditions in the respective treatment indicating stimulus-specific pathways in stress-induced macroautophagy.

DOI: https://doi.org/10.1080/15548627.2016.1274485

Influenza A virus induces autophagosomal targeting of ribosomal proteins

Andrea C. Becker[1,2], Monique Gannagé[3], Sebastian Giese[2,4], Petra Paul[5], Lea Bühler[1,2], Zehan Hu[1,2,7], Christine Gretzmeier[1,2], Veronica I. Dumit[6], Martin Schwemmle[2,4], Christian Münz[5], and Jörn Dengjel[1,2,7,#]

[1]Department of Dermatology, Medical Center University of Freiburg, Hauptstr. 7, 79104 Freiburg, Germany

[2]Faculty of Medicine, University of Freiburg, Breisacher Strasse 153, 79110 Freiburg, Germany

[3]Department of Pathology and Immunology, School of Medicine, University of Geneva, 1 rue Michel Servet, 1211 Geneva, Switzerland

[4]Institute for Virology, Medical Center, University of Freiburg, Hermann-Herder-Strasse 11, 79104 Freiburg, Germany

[5]Viral Immunobiology, Institute of Experimental Immunology, University of Zurich, Winterthurerstrasse 190, 8057 Zürich, Switzerland

[6]Core Facility Proteomics, Center for Biological Systems Analysis (ZBSA), University of Freiburg, Habsburgerstr. 49, 79104 Freiburg, Germany

[7]Department of Biology, University of Fribourg, Chemin du Musée 10, 1700 Fribourg, Switzerland

Running title: Autophagosomal targeting of ribosomal proteins by IAV

Correspondence to:

Jörn Dengjel, Department of Biology, University of Fribourg, Chemin du Musée 10, 1700 Fribourg, Switzerland; Email: joern.dengjel@unifr.ch

Abbreviations

BH: Benjamini-Hochberg

conA: concanamycin A

GFP: green fluorescent protein

IAV: influenza A virus

IF: immunofluorescence

LC: liquid chromatography

MS: mass spectrometry

MOI: multiplicity of infection

PAMP: pathogen-associated molecular pattern

PFU: plaque-forming unit

SILAC: stable isotope labelling by amino acids in cell culture

vRNPs: viral ribonucleoprotein complexes

WB: western blot

Summary

Seasonal epidemics of influenza A virus in the human population are a major cause of severe illness and are of high socio-economic relevance. For the design of effective anti-viral therapies, a detailed knowledge of cellular pathways perturbed by virus infection is critical. We performed comprehensive expression and organellar proteomics experiments to identify new protein targets and cellular pathways affected by influenza A virus. Type I as well as type II interferon pathways were upregulated upon infection, affecting amongst others poly ADP-ribose polymerase transcription factors and ubiquitin-like modifiers. Interestingly, influenza A virus had also a major influence on the subcellular localization of proteins and complexes. In virus-infected cells, the vesicular compartment appeared expanded and in particular, the composition of autophagsomes was altered by targeting of ribosomes to these vesicular organelles, next to viral mRNA. Thus, autophagy may support viral protein translation by clustering of the critical cellular components.

Keyword: proteomics, mass spectrometry, influenza, virus, organelle, autophagy, vesicle, ribosome, autophagosome

Introduction

Influenza virus infections of the human respiratory tract are a major cause of morbidity and mortality (1). Seasonal epidemics mainly affect young, elderly, or chronically ill people and are estimated to result in up to 5 million cases of severe illness, including up to 500`000 fatal outcomes (1). In addition to the annual outbreaks, the rarely occurring influenza A virus (IAV) pandemics, such as the “Spanish Flu” in 1918-1919, gave rise to tens of millions of deaths worldwide (2). Periodic influenza epidemics occur as a result of an accumulation of mutations in the viral surface protein hemagglutinin of influenza viruses circulating in the human population to escape the humoral immune response. IAV reassortant viruses, harboring a “new” hemagglutinin where no preexisting immunity exist, may cause pandemics.

Due to the high mutation rates of viral RNA, therapies based on anti-viral drugs targeting virally encoded proteins themselves have likely only limited effects (3). Hence, understanding of the host factors critical for viral replication is regarded as a powerful alternative to characterize new target processes accessible for interference with viral replication. Several genome-wide RNAi screens were performed to identify host factors necessary for IAV replication (4-6). In parallel, global mass spectrometry (MS)-based proteomics studies were also performed to identify such factors. These analyses focused either on the identification and characterization of host-virus protein interactions (7,8), or on the analyses of IAV-induced changes in host protein abundances (9-11). In the current study, we aimed at comprehensively characterizing IAV-induced changes in the host cell proteome by not only quantifying differences in protein abundances, but also by characterizing the dynamic, IAV-induced regulation of the subcellular localization of proteins complexes.

During its replication cycle, IAV modifies and hijacks numerous processes and cell organelles. After endocytic cell entry, viral ribonucleoprotein complexes (vRNPs) are released into the cytoplasm and enter the nucleus where viral mRNA synthesis and replication occurs (12,13). A cell process utilized by IAV that has recently attracted attention is autophagy, a catabolic recycling process that targets organelles and multiprotein complexes for lysosomal degradation (14). IAV

blocks the maturation of autophagosomes (15), which are double membrane vesicles that shuttle intracellular cargo to lysosomes. The autophagic membranes are further redirected to the plasma membrane to enable the release of viral particles with increased stability (16).

Here, we present expression proteomics and organellar proteomics data, highlighting the multifaceted influences of IAV on human proteome composition and configuration. We characterize signaling pathways and new molecular players regulated by IAV infection and analyze the cellular redistribution of host protein complexes. Specifically, we study the impact of IAV on the vesicular proteome, mainly autophagosomes, highlighting a potential new role of these organelles in virus replication.

Experimental Procedures

Cells and culture conditions

Adherent human A549 were cultured and passaged in high glucose DMEM (PAA Laboratories GmbH, Coelbe, Germany), supplemented with 10% FBS, 1% Penicillin/Streptomycin and 1% L-glutamine. For SILAC-labeling, cells were grown in SILAC-DMEM (high glucose) (Thermo-Fisher scientific, Langenselbold, Germany), supplemented with 10% dialyzed FBS (Invitrogen, Darmstadt, Germany), 1% Penicillin/Streptomycin and 1% L-glutamine, containing a final concentration of 42 mg/l L-arginine HCl, 73 mg/l L-lysine HCl and 1.33 mg/l L-proline for light labeling (Sigma-Aldrich, Taufenkirchen, Germany), L-arginine-$^{13}C_6{}^{14}N_4$ and L-lysine-$^{2}H_4$ (Arg6, Lys4) and 1.33 mg/l L-proline for medium heavy, or L-arginine-$^{13}C_6$-$^{15}N_4$ and L-lysine-$^{13}C_6{}^{15}N_2$ (Arg10, Lys8) and 1.33 mg/l L-proline for heavy labeling (Silantes, München, Germany). To gain full incorporation of labeled amino acids, cells were cultured for at least 5 cell doublings in the corresponding label. For harvesting, cells were washed 3 times with ice cold DPBS, collected with a cell scraper, centrifuged at 1000 g for 5 min and cell pellets were stored at -80°C until use.

Experimental Design and Statistical Rationale

We minimally analyzed two biological replicates from all conditions and correlations of respective data are shown in the supplemental information. Values of biological replicates were combined as average and log2 transformed to generate normal distributions. All statistical tests were corrected for multiple testing as outlined in the respective paragraphs.

IAV infection

Cells (60-70% confluence) were washed twice with RPMI (PAA Laboratories) and incubated with influenza virus strain X:31 A/AICHI/68 (Charles River, Wilmington MA; Batch: 4XAP091028) in RPMI at a multiplicity of infection (MOI) of 2 PFU per cell (for IF staining a MOI of 4 was used) for

1h at 37°C with 5% CO_2. Cells were washed once with DPBS and incubated with complete DMEM (high glucose) for 24 hours.

Cell fractionation

Cell pellets were solved in homogenization medium (HM; 0.25 M Sucrose, 1 mM EDTA, 20 mM HEPES-NaOH pH 7.4), containing protease inhibitor (Complete protease inhibitor cocktail, Roche Diagnostics GmbH, Mannheim, Germany). The solution was dounced 150 times followed by several centrifugation steps to collect nuclear (1,000 g), mitochondrial (3,000 g) and vesicular fractions (17,000 g). The supernatant after the last centrifugation was collected as the cytosolic fraction. All pellets were resuspended in HM and centrifuged for a second time at the respective speed.

The mitochondrial and vesicular fractions were resuspended in modified RIPA buffer (1% NP-40, 150 mM NaCl, 50 mM Tris pH 7.5, 0.25% Na-deoxycholate) and incubated on ice for 10 min followed by a centrifugation for 10 min at 17,000 g at 4°C.

The nuclear pellet was solved in 3 ml of S1 (0.25 M Sucrose, 10 mM $MgCl_2$). This solution was layered over 3 ml of S2 (0.35 M Sucrose, 0.5 mM $MgCl_2$), and passed through at 1,430 g for 5 min at 4°C. The pellet was again solved in 3 ml S1 and the first step was repeated. The nuclear pellet was solved in modified RIPA buffer and the nuclei were opened by sonification (3x 30 sec with 50% intensity in an ultrasonic bath, kept at ice in between), followed by a centrifugation at 3,000 g for 10 min at 4°C. The supernatant contains the nucleoplasmic fraction. The protein amount of all collected fractions was determined (BCA Protein Assay kit, PierceR, Thermo-Fisher scientific) according to the manufacturer`s protocol, adjusted and the fractions were further processed for MS or western blot.

Autophagosome purification by protein correlation profiling

Cell pellets were treated as outlined above. The 17,000 g pellet containing the vesicular fraction was resuspended in 1 ml HM and loaded on top of an iodixanol gradient (Sigma Aldrich). The gradient was made of five 1.6 ml gradient steps (5, 10, 16, 24 and 30% iodixanol in HM), prepared by underlying layers with higher density solutions in 12 ml centrifugation tubes. Vesicles were separated on the gradient for 17 h at 100,000 g at 6 °C in a swing out rotor. Fractions of 1 ml were collected, diluted with 1 ml HM and centrifugated at 4°C for 20 min at 40,000 g in a fixed angle rotor. Pellets were solved in 25 µl SDS-PAGE loading buffer and further processed for MS or western blot (17).

Protease protection assay

The vesicular fraction, gained by differential centrifugation was used to perform the protease protection assay. The vesicular pellet was solved in HM and split into 5 tubes. One sample was left untreated, two were treated with 40 µg/ml and 80 µg/ml proteinase K respectively and two were treated with 0.2% triton and 40 µg/ml and 80 µg/ml proteinase K, respectively. Samples were vortexed and incubated for 30 min on ice. 7% TFA was used in order to stop the enzyme activity. The precipitated proteins were pelleted via centrifugation for 10 min at 4°C at 21`100 g and washed twice with acetone. 1 x SDS-loading buffer containing 1 mM DTT was added and the samples were brought into solution by heating them up to 65°C for 30 minutes.

Western blot

Samples were mixed with SDS-PAGE loading buffer with 1 mM DTT and incubated for 10 min at 95°C. After that, proteins were separated on SDS-PAGE on self-casted SDS-gels (dependent on protein size, gels between 7.5% and 12.5% were used) and transferred onto a nitrocellulose membrane. The membranes were blocked with 5% milk powder in 1x TBS with 0.1% Tween-20 for 1 h at room temperature and incubated for 1 h at room temperature or overnight at 4°C with

primary antibodies. HRP-coupled secondary antibodies and a chemiluminescent detection assay were used for visualization according to manufacturer`s instructions.

Following primary antibodies were used. Santa Cruz Biotechnology, Inc., Heidelberg, Germany: Anti-beta-actin (sc-47778), Anti-DTX3L (sc-100627), Anti-EEA1 (G-4, sc-137130), Anti-GFP (B-2, sc-9996), Anti-Influenza A NS1 (NS1-23-1, sc-130568), Anti-PARP14 (sc-377150), Anti-Ribosomal Protein L4 (RQ-7, sc-100838), Anti-Tom20 (F-10, sc-17764), Anti-UBC8 (sc-135629). Abcam, Cambridge, United Kingdom: Anti-beta-tubulin (ab6046), Anti-MCM7 (47DC141). Roche: Anti-HA (11867423001). Cell Signaling Technology, Inc., Danvers, MA, USA: Anti-Lamin A/C (2032), Anti-LC3 A/B (4108). Biomol: Anti-p62/SQSTM1 (PW 986). Merck, Darmstadt, Germany: Anti-GAPDH (MAB374).

Following secondary antibodies were used. Thermo-Fisher Scientific: Alexa fluor 488 (A21042), Alexa fluor 488 (A21206), Alexa fluor 568 (A11011), Alexa fluor 568 (A10037). GE Healthcare, München, Germany: Anti-rabbit HRP (NA934V), Anti-mouse HRP (NXA931). Dianova GmbH, Hamburg, Germany: Anti-rat HRP (112-035-062).

Calculation of autophagic flux

The intensity gained by western blot was measured using imageJ analysis software and the level of LC3-II was normalized to GAPDH as a loading control. Autophagic flux was calculated as intensity of LC3-II with conA divided by intensity of LC3-II without conA. The additional accumulation of LC3-II under conA treatment with infection (conA+FluA) was compared to the level of infection (FluA) only. The same was done for conA only treated cells compared to untreated control cells. The level of conA /untreated was set to 100% and the (conA+FluA)/FluA was adjusted accordingly.

Immunofluorescence staining

For indirect immunofluorescence staining, A549 cells were grown on coverslips, fixed with 4% PFA and blocked with 1% BSA in PBS for 30 min at room temperature. Incubation with primary antibodies diluted in 1% BSA in PBS was performed for 1 h at room temperature or overnight at 4°C. After incubation with the fluorophore-coupled secondary antibody in 1% BSA in PBS for 1 h, the samples were embedded in fluorescence mounting medium, containing DAPI. Pictures were taken with an IF microscope.

RNA purification, cDNA synthesis and PCR conditions

For RNA purification, cell pellets or pellets of the vesicular fraction after gradient centrifugation were extracted with the RNeasy Mini kit following the manufacturer`s instructions using the RLT buffer. Dependent on the experiments, 1 µg of total RNA was reverse transcribed using the First Strand cDNA Synthesis Kit with random hexamer primers. PCR primer : M1, ATGAGTCTTCTAACCGAGG, TCACTTGAACCGTTGCATC ; NS1, ATGGATCCAAACACTGTGTC, TCAAACTTCTGACCTAATTGTT.

MS sample preparation

Samples were lysed in SDS-PAGE loading buffer, reduced with 1 mM DTT for 10 min at 95°C and alkylated using 5.5 mM iodacetamide for 30 min at 25°C in the dark. Proteins were separated by SDS-PAGE using 4-12% Bis-Tris gels (NuPAGE, Invitrogen, Darmstadt, Germany). Staining with Colloidal Blue was used to visualize the proteins. The gel lanes were cut into 10 slices of equal size, which were cut into small cubes. Remaining Colloidal Blue was washed out by incubation with ABC buffer (100 mM ammonium bicarbonate pH 7.5) for 10 min followed by incubation for 10 min in ethanol. This was repeated for three times. 12.5 ng/µl trypsin (MS grade, Promega, Mannheim, Germany) was added and incubated for digestion over night at 37°C. Trypsin activity was stopped by acidification with 0.5% TFA. Remaining peptides were washed out of the gel cubes by two times incubation in 100 µl ethanol and the supernatant of the respective slice was

combined. The peptide solution was concentrated to less than 50 µl in a speedvac to remove ethanol. Samples were desalted on STAGE tips (18).

Mass spectrometry

Samples were fractionated by nanoscale HPLC on either a 1200 (Agilent Technologies; Waldbronn, Germany) or a NanoLC Ultra (Eksigent, AB SCIEX, Redwood City, CA, USA) connected online to a LTQ Orbitrap XL mass spectrometer (Thermo Fisher Scientific, Bremen, Germany). Fused silica HPLC-column tips with 75 µm inner diameter were self-packed with Reprosil–Pur 120 ODS–3 (Dr. Maisch, Ammerbuch, Germany) to a length of 20 cm. Samples were directly injected into the mass spectrometer by applying a linear gradient from 10–30% acetonitrile in 0.5% acetic acid with a flow rate of 250 nl/min and for sample application 500 nl/min. The spray voltage was set to 2.3 kV and the ion-transfer tube had a temperature of 125°C. All full-scan were recorded in the Orbitrap in the range from m/z 370 to 2,000 and at resolution 60,000. MS/MS scans were recorded in the linear ion trap and the top5 method was applied. The normalized collision energy was set to 35% at a target value of 5,000. Singly charged and ions with unassigned charge state were excluded from MS/MS.

Identification of proteins and protein ratio assignment using MaxQuant

The MS raw data files were uploaded into the MaxQuant software (version 1.2.2.5, 1.3.0.5) (19). Database searches were performed against a homemade full-length human database containing common contaminants such as keratins and enzymes used for in–gel digestion as well as IAV protein sequences (87`093 entries). Carbamidomethylcysteine was set as fixed modification, oxidation of methionine and protein amino–terminal acetylation was set as variable modifications. Dependent on the experiment, double or triple SILAC was used as quantitation mode. The enzyme specificity was trypsin/P+DP with three allowed miss cleavages. The MS/MS tolerance was set to 0.5 Da and the mass precision of identified peptides after recalibration was in general less than 1

ppm. For identification and quantitation, the following settings were used: peptide and protein FDR were set to 0.01, maximum peptide posterior error probability (PEP) was set to 0.1, minimum peptide length was set to 7, minimum number peptides for identification and quantitation of proteins was set to two of which one must be unique, minimum ratio count was set to two, and only unmodified peptides and the variable modification were used for protein quantification. The "match between run" option was used with a time window of 2 min.

MS raw data have been deposited to the ProteomeXchange Consortium via the PRIDE partner repository (20). Project Name: Influenza A virus induces autophagosomal targeting of ribosomal proteins; Project accession: PXD007809; Reviewer account details: Username: reviewer13476@ebi.ac.uk; Password: PuVBwX6A

Data analysis

For clustering of data, all proteins with ratios in all six gradient fractions or in all four compartments were used to generate respective distribution profiles by applying the fuzzy c-means clustering (21) using R 2.8.1 or GProX (22). To address the biological implications of the proteins in each cluster, Biological Process and Molecular Function GO terms were retrieved using Perseus (23). A Fisher`s exact test was performed to identify enriched GO terms in the corresponding cluster, compared to the background of the same sample over all cluster. A Benjamini-Hochberg FDR below 0.01, an enrichment factor of 2 and a membership of at least five per GO term in the cluster were required to regard the enrichment as significant. Additionally, all proteins of a cluster were tested for known and predicted interactions by using STRING (24). Cytoscape was used for visualization and network analysis (25).

Results

Characterization of IAV-induced changes in the composition of the host cell proteome

To determine the effect of IAV infection on the composition of the host cell proteome, we chose a quantitative expression proteomics approach based on SILAC labeling, analyzing both, whole cell lysate (WCL) as well as major organelle fractions to achieve a deep proteomic coverage (Figure 1A). Briefly, A549 human lung epithelial carcinoma cells were differentially SILAC labeled and either left untreated as control or infected for 24 h with IAV strain X:31 (A/AICHI/68) with an MOI of 2. WCL, nuclear, mitochondrial, vesicular and cytosolic cell fractions were mixed 1:1, respectively, and analyzed as outlined (Figure 1A, Supplemental Figure S1). In two biological replicates each (Supplemental Figure S2, average Pearson correlation coefficient r = 0.54), we identified 4`513 proteins, of which we could quantify 3`778 by minimally two peptides (Supplemental Table S1). Fold changes comparing IAV infected versus untreated control cells were used to identify significantly regulated host cell proteins upon IAV treatment (Figure 1B, Supplemental Figure S3). In total, we identified 236 proteins, which exhibited a significantly changed abundance (Supplemental Table S2). Various proteins known to play a role in the “influenza A virus” life cycle were significantly enriched (KEGG, FDR=7.98e-05). Out of these 236 candidates, 20 proteins were shown to interact with IAV proteins and to be critical for viral replication (7). Additionally, 20 proteins were also identified as being regulated by IAV in two other recent MS-based proteomics studies (9,10) (see Supplemental Table S3 for hits commonly identified by other studies).187 of the regulated proteins formed an interaction network based on STRING DB indicating a functional connection between regulated proteins after infection (Figure 1C) (24). Amongst others, interacting proteins were significantly enriched in proteins of the “type I interferon signaling pathway” (GO BP, FDR=3.66e-20), such as IFN-induced IFIT1, IFIT2 and IFIT3, which belong to the same gene family, IFIT1 being known to act as a sensor for viral single-

stranded RNA (26) (see Supplemental Tables S4-S7 for complete GO BP, MF, CC and KEGG enrichments).

We validated increased abundance after IAV infection of three proteins by western blot (WB) and immunofluorescence (IF) analysis, which were so far not known to be regulated by IAV. The poly [ADP-ribose] polymerase transcription factor PARP14, which was described to be important for T cell differentiation into Th2, Th17 and Tfh cells (27,28), was shown by WB to be more abundant after virus infection (Figure 1D). Next to PARP14, we also identified PARP9, 10 and 12 as upregulated indicating a broader effect of IAV infection on this family of transcription factors (Supplementary Table S2). The increased abundance of the E3 ubiquitin ligase DTX3L involved in DNA damage responses was validated by IF (Figure 1E) (29). Finally, the E2 ubiquitin-conjugating enzyme UBE2L6 was reproducibly identified as slightly upregulated by WB and IF (Figure 1D-E). UBE2L6 is the E2 enzyme of ISG15, which is known to be involved in the anti-IAV host response (30). Interestingly, also HERC5, the respective E3 enzyme, was identified as significantly enriched (Supplementary Table S2). Thus, IAV infection induced a potent host cell response affecting known (31) as well as new pathways potentially critical in anti-viral host cell signaling.

IAV-induced changes in subcellular localization of host proteins

In a comprehensive study addressing human cytomegalovirus, it was shown that viral proteins change the subcellular localization of numerous host cell proteins (32). To study the influence of IAV on subcellular protein localization, we performed experiments based on a PCP-SILAC setup (33). In a triple labeling approach, we fractionated IAV and untreated cells into vesicular, nuclear, mitochondrial and cytosolic compartments (Figure 2A). Light-labeled fractions were combined and served as an internal standard, spiked in a 1:1:1 ratio into mixed fractions of medium-heavy and heavy labeled cells. This allowed the generation of protein fractionation profiles by LC-MS/MS and the identification of IAV-induced changes in the subcellular localization of proteins (ratio

heavy/light over all compartments compared to ratio medium-heavy/light over all compartments). Average ratios of two biological replicates were used to generate 1`858 protein profiles (Supplemental Table S8), which were analyzed by fuzzy c-means clustering (Figure 2B) (21,22). Profiles separated into eight clusters of similar size and a GO term-enrichment analysis was performed to detect enriched protein groups in each cluster (Figure 2C). As expected, clusters and GO terms reflected the cell fractionation approach, e.g. cluster 1 and 2 protein profiles peak in the mitochondrial fraction, which is mirrored by the enriched GO terms.

We identified four complexes/processes that changed subcellular localization due to IAV treatment: the proteasome regulatory complex, the MCM complex, translation initiation and elongation, and the ribosome (Figure 2C). Respective GO terms were enriched in clusters 7 and 8 under control conditions and changed to clusters 3 and 7 upon IAV infection, respectively. The MCM complex, a DNA replicative helicase, appeared to shift from the nuclear to the vesicular fraction under infection (Figure 2D). Indeed, MS-based quantification of MCM proteins in the nuclear fraction revealed a significant decrease in IAV treated cells (Figure 2E), which was also observed by IF analysis of the subunit MCM7 (Figure 2F). This indicated a reduced ability of IAV infected cells to initiate host genome replication, potentially impairing cell proliferation. In parallel ribosomal proteins, as exemplified by fractionation profiles of large ribosomal subunit proteins (Figure 2G), appeared to be more abundant in the vesicular fraction upon IAV infection. WB analysis of the ribosomal protein RPL4 in the vesicular fraction confirmed a significant increase in IAV treated cells (Figure 2H, $p<0.01$, $n=3$). As the majority of changes in cellular configuration and organization of protein complexes seemed to occur in the vesicular fraction and IAV was shown to interfere with intracellular vesicle trafficking, in particular autophagy (15), we decided to focus further analyses on to the vesicular fraction.

IAV-induced changes of the autophagosomal proteome

IAV was shown to interfere with lysosomal targeting of autophagosomes and to lead to autophagosome accumulation (for review see (14)). However, it is still under debate whether IAV infection blocks maturation or rather induces functional autophagy, which ultimately leads to an accumulation of autophagosomes (15,34). Before continuing the analysis of the vesicular proteome in IAV treated cells, we analyzed the consequences of IAV treatment on lysosomal targeting of autophagosomes in our experimental system. We used A549 cells stably expressing the autophagosomal marker protein MAP1LC3B (LC3-II) fused to GFP. Upon IAV treatment, we observed an accumulation of autophagosomes by IF to a similar extent as by blocking lysosomal acidification/degradation by concanamycin A (conA, Figure 3A). Next, we analyzed autophagy flux by WB comparing the band intensities of the autophagy receptor SQSTM1 and of LC3-II in the presence and absence of conA and IAV, respectively (Figure 3B-C) (35). In agreement with a block of autophagosomal-lysosomal fusion (15), we detected a decreased autophagy flux in our experimental conditions. Thus, IAV infection results in an autophagy block, an accumulation of autophagosomes and accordingly in an expansion of the vesicular compartment.

To study the regulation of the vesicular proteome by IAV, again a PCP-SILAC-based approach was chosen (Figure 4A, Supplemental Tables S9-S10) (17,36). Cells were lysed by dounce homogenization, the vesicular fraction was enriched by differential centrifugation and separated by gradient centrifugation. Six fractions were collected and proteins therein analyzed by WB and LC-MS/MS. Protein gradient profiles of conA-treated cells, which leads to a block of constitutive autophagy, were compared to IAV treated cells. In agreement to published data, in both conditions autophagosomes were fractionated as described (15,36), and as controlled by WB analysis of GFP-linked LC3-II (Figure 4B). Corroborating the finding that IAV localizes to autophagosomes (15), we identified all viral proteins as co-migrating with the autophagosomal marker proteins LC3 and GABARAPL (Figure 4C). To study vesicular proteomes unbiasedly, protein profiles were again clustered and the potential autophagosomal cluster was identified by known marker proteins (LC3, GABARAPL, SQSTM1; Supplemental Figure S4, n=2). In IAV treated cells,

autophagosomes appeared to be more heterogeneous, as marker proteins spread over two related clusters. A GO term enrichment analysis of potential autophagosomal proteins was performed, clearly discriminating the two treatments (Figure 4D). Whereas in conA-treated cells autophagosomes appeared to contain mostly lysosomal and endosomal proteins, IAV treatment led to an accumulation of ribosomal proteins and proteins involved in viral infection in autophagosomal clusters.

IAV-induced accumulation of ribosomes inside autophagosomes

As GO term enrichment analysis indicated a virus-dependent, increased localization of ribosomal proteins within autophagosomes, we studied a potential ribosome-autophagosome crosstalk in IAV treated cells. Indeed, in contrast to conA-treated cells, proteins of the large ribosomal subunit closely followed autophagosomal marker proteins in gradient centrifugations of IAV treated cells (Figure 5A). Co-migration in gradient centrifugations could mean both, association with or uptake by autophagosomes. This question was addressed biochemically using a proteinase K protection assay (37), which enables the discrimination between truly (intra)organellar proteins and associated proteins not inside vesicles by performing digestion assays in the absence and presence of detergent (Figure 5B). Whereas soluble GFP-LC3-I was degraded by proteinase K in the presence and absence of detergent, the autophagy receptor SQSTM1 and membrane-bound GFP-LC3-II, both mainly localizing inside autophagosomes, were protease resistant in the absence of detergent. Under control conditions, a minor protease resistant band of the ribosomal protein RPL4 was detected. However, this was similar to the observed GFP-LC3-I bands indicating that under control conditions ribosomes might only co-migrate with autophagosomes, in agreement with earlier studies (36). Under IAV infection, autophagosomes appeared to be more fragile, as partial digestion of GFP-LC3-II and SQSTM1 could be observed in the absence of detergent (Figure 5B). Importantly however, RPL4 was relatively protease resistant in the absence

of detergent, leading to a significant increase of the ribosomal protein inside autophagosomes under IAV treatment (Figure 5C).

To test if in addition to viral proteins and ribosomes, viral mRNA could be a cargo of autophagosomes, RNA was isolated from gradient fractions. Primers for mRNA encoding viral *M1* and *NS1* and for the human housekeeping genes *18S* and *HPRT1* were used to determine the mRNA content of the vesicular gradient fractions by PCR (Figure 5D). Whereas it was not possible to detect mRNA of the human housekeeping genes (data not shown), viral mRNA showed a similar gradient profile as viral proteins. Thus, in addition to ribosomes and viral proteins, viral mRNA appeared to localize to autophagosomes.

Discussion

As IAV infects epithelial cells of the lung (38), we used the lung epithelial cancer cell line A549 to study the response of the host cell proteome to IAV infection. We analyzed protein abundance changes as well as IAV-induced changes in subcellular protein localization, identifying pleiotropic effects and shedding light on processes so far not known to be regulated by IAV.

We could show that IAV positively regulated the abundance of proteins involved in the class I IFN response, corroborating literature knowledge (39). Importantly, we also characterized so far unknown molecular details. Whereas the antiviral effects of the ubiquitin-like modifier ISG15 were well known (30,40), we could show that the respective E2 enzyme UBE2L6 and the E3 ligase HERC5 were upregulated on protein level, potentially being causative for the increased modification of viral NS1 by ISG15. Upon IAV treatment, we also identified increased abundance of the transcription factors PARP9, 10, 12 and 14, which belong to the same family of macroPAMPs (pathogen-associated molecular patterns) and are implicated in immune activation. The expression of PARP9 was shown to be induced by IFNγ, which is also triggered by IAV, and expression of PARP9 in lymphoma cells was found to increase the expression of several interferon-stimulated genes (41). PARP14 is involved in the transcriptional activation of the *IL4* gene and may promote an inflammatory response. To our knowledge, both PARP9 and 14 were so far not found to be upregulated by virus infection. PARP9 and the E3 ubiquitin-protein ligase DTX3L, which was also identified as increased, are located in a head-to-head orientation on chromosome 3q21 and are regulated by an IFNγ-responsive bidirectional promoter (42). DTX3L binds to PARP9 and regulates its subcellular localization, highlighting a coordinated, IAV-dependent expression of PARP9 and DTX3L in A549 cells.

Next to changes in protein abundance, IAV also affected the subcellular localization of host proteins. Whereas MS-based proteomics approaches were used in the past to study the effects of influenza virus on organellar proteomes, amongst others nucleus, nucleolus, mitochondrion and cytosol (43-45), a detailed analysis on the underlying dynamics was missing. To our knowledge,

this is the first attempt to globally analyze IAV-induced changes in cellular protein localization. The majority of changes in cellular reorganization of protein complexes seemed to affect the vesicular fraction, possibly highlighting the block of autophagosomal maturation by IAV (15). We could show that the MCM complex was less abundant in nuclei of IAV infected cells and appeared to accumulate in the vesicular fraction. It was shown that the MCM complex is important for viral replication stabilizing the replication polymerase complex by promoting the interaction between influenza polymerase and nascent cRNA (46). However, this complex was thought to form inside nuclei. Our data raises the question if this complex could be exported from the nucleus by vRNPs, and also play a role in vesicles?

A second complex, which appeared to accumulate in the vesicular fraction upon IAV treatment, was the ribosome. As both, IAV and ribosomal proteins may localize to autophagosomes (15,47,48), we analyzed autophagy and autophagosomal protein content in IAV treated cells in detail. In the chosen experimental system, IAV blocked autophagosome maturation and hence we compared autophagosomes accumulation following IAV infection to autophagosomes accumulated by conA treatment, representing autophagosomes under basal conditions (36). Autophagosomes appeared to be more heterogeneous and fragile under IAV treatment as indicated by gradient profiles of respective marker proteins and decreased stability in protease protection assays. This could be due to the fact that IAV leads to a redirection of autophagic membranes to the plasma membrane and the site of IAV budding (16). We biochemically characterized that ribosomal proteins are inside autophagosomes upon IAV treatment, and that viral mRNA appears to be taken up by autophagosomes as well. Together with the localization of viral proteins inside autophagosomes (15), this opens up the possibility that active viral protein biosynthesis might happen inside autophagosomes. Whether this is of physiological importance remains elusive. Whereas it has been reported by several laboratories that autophagy incompetent cells produce less viral proteins, an effect on viral titer was not found (15,49).

However, recently a time-dependent effect of autophagy levels on IAV titer was described (50). Our findings could highlight the cell biological reasons for these phenotypic observations.

Taken together, by a comprehensive MS-based proteomics approach we identified IAV-dependent changes in host cell protein abundances as well as localizations, and characterized the autophagosome as a potential organelle in which viral protein translation may take place.

Acknowledgements

We wish to thank Jan Riemer for technical advice with the protease protection assay and Martin Biniossek for technical assistance with a mass spectrometer. This work was supported by the Swiss National Science Foundation, grant 31003A-166482/1, by TRANSAUTOPHAGY, COST Action CA15138, and by the Alexander von Humboldt Foundation (to JD).

References

1. WHO. (2016) Influenza (Seasonal) Fact sheet.
2. Taubenberger, J. K., and Kash, J. C. (2010) Influenza virus evolution, host adaptation, and pandemic formation. *Cell Host Microbe* **7**, 440-451
3. Neumann, G., Noda, T., and Kawaoka, Y. (2009) Emergence and pandemic potential of swine-origin H1N1 influenza virus. *Nature* **459**, 931-939
4. Konig, R., Stertz, S., Zhou, Y., Inoue, A., Hoffmann, H. H., Bhattacharyya, S., . . . Chanda, S. K. (2010) Human host factors required for influenza virus replication. *Nature* **463**, 813-817
5. Brass, A. L., Huang, I. C., Benita, Y., John, S. P., Krishnan, M. N., Feeley, E. M., . . . Elledge, S. J. (2009) The IFITM proteins mediate cellular resistance to influenza A H1N1 virus, West Nile virus, and dengue virus. *Cell* **139**, 1243-1254
6. Karlas, A., Machuy, N., Shin, Y., Pleissner, K. P., Artarini, A., Heuer, D., . . . Meyer, T. F. (2010) Genome-wide RNAi screen identifies human host factors crucial for influenza virus replication. *Nature* **463**, 818-822
7. Watanabe, T., Kawakami, E., Shoemaker, J. E., Lopes, T. J., Matsuoka, Y., Tomita, Y., . . . Kawaoka, Y. (2014) Influenza virus-host interactome screen as a platform for antiviral drug development. *Cell Host Microbe* **16**, 795-805
8. Heaton, N. S., Moshkina, N., Fenouil, R., Gardner, T. J., Aguirre, S., Shah, P. S., . . . Marazzi, I. (2016) Targeting Viral Proteostasis Limits Influenza Virus, HIV, and Dengue Virus Infection. *Immunity* **44**, 46-58
9. Coombs, K. M., Berard, A., Xu, W., Krokhin, O., Meng, X., Cortens, J. P., . . . Brown, E. G. (2010) Quantitative proteomic analyses of influenza virus-infected cultured human lung cells. *J Virol* **84**, 10888-10906
10. Sadewasser, A., Paki, K., Eichelbaum, K., Bogdanow, B., Saenger, S., Budt, M., . . . Wolff, T. (2017) Quantitative Proteomic Approach Identifies Vpr Binding Protein as Novel Host Factor Supporting Influenza A Virus Infections in Human Cells. *Mol Cell Proteomics* **16**, 728-742
11. Mindaye, S. T., Ilyushina, N. A., Fantoni, G., Alterman, M. A., Donnelly, R. P., and Eichelberger, M. C. (2017) Impact of Influenza A Virus Infection on the Proteomes of Human Bronchoepithelial Cells from Different Donors. *J Proteome Res* **16**, 3287-3297
12. Das, K., Aramini, J. M., Ma, L. C., Krug, R. M., and Arnold, E. (2010) Structures of influenza A proteins and insights into antiviral drug targets. *Nat Struct Mol Biol* **17**, 530-538
13. Eisfeld, A. J., Neumann, G., and Kawaoka, Y. (2015) At the centre: influenza A virus ribonucleoproteins. *Nat Rev Microbiol* **13**, 28-41
14. Paul, P., and Munz, C. (2016) Autophagy and Mammalian Viruses: Roles in Immune Response, Viral Replication, and Beyond. *Adv Virus Res* **95**, 149-195

15. Gannage, M., Dormann, D., Albrecht, R., Dengjel, J., Torossi, T., Ramer, P. C., . . . Munz, C. (2009) Matrix protein 2 of influenza A virus blocks autophagosome fusion with lysosomes. *Cell Host Microbe* **6**, 367-380
16. Beale, R., Wise, H., Stuart, A., Ravenhill, B. J., Digard, P., and Randow, F. (2014) A LC3-interacting motif in the influenza A virus M2 protein is required to subvert autophagy and maintain virion stability. *Cell Host Microbe* **15**, 239-247
17. Becker, A. C., and Dengjel, J. (2014) Autophagosomal proteome analysis by protein correlation profiling-SILAC. *Methods Mol Biol* **1188**, 271-279
18. Rappsilber, J., Mann, M., and Ishihama, Y. (2007) Protocol for micro-purification, enrichment, pre-fractionation and storage of peptides for proteomics using StageTips. *Nat Protoc* **2**, 1896-1906
19. Cox, J., and Mann, M. (2008) MaxQuant enables high peptide identification rates, individualized p.p.b.-range mass accuracies and proteome-wide protein quantification. *Nat Biotechnol* **26**, 1367-1372
20. Vizcaino, J. A., Csordas, A., del-Toro, N., Dianes, J. A., Griss, J., Lavidas, I., . . . Hermjakob, H. (2016) 2016 update of the PRIDE database and its related tools. *Nucleic Acids Res* **44**, D447-456
21. Futschik, M. E., and Carlisle, B. (2005) Noise-robust soft clustering of gene expression time-course data. *J Bioinform Comput Biol* **3**, 965-988
22. Rigbolt, K. T., Vanselow, J. T., and Blagoev, B. (2011) GProX, a user-friendly platform for bioinformatics analysis and visualization of quantitative proteomics data. *Mol Cell Proteomics* **10**, O110 007450
23. Tyanova, S., Temu, T., Sinitcyn, P., Carlson, A., Hein, M. Y., Geiger, T., . . . Cox, J. (2016) The Perseus computational platform for comprehensive analysis of (prote)omics data. *Nat Methods* **13**, 731-740
24. Szklarczyk, D., Morris, J. H., Cook, H., Kuhn, M., Wyder, S., Simonovic, M., . . . von Mering, C. (2017) The STRING database in 2017: quality-controlled protein-protein association networks, made broadly accessible. *Nucleic Acids Res* **45**, D362-D368
25. Shannon, P., Markiel, A., Ozier, O., Baliga, N. S., Wang, J. T., Ramage, D., . . . Ideker, T. (2003) Cytoscape: a software environment for integrated models of biomolecular interaction networks. *Genome Res* **13**, 2498-2504
26. Pichlmair, A., Lassnig, C., Eberle, C. A., Gorna, M. W., Baumann, C. L., Burkard, T. R., . . . Superti-Furga, G. (2011) IFIT1 is an antiviral protein that recognizes 5'-triphosphate RNA. *Nat Immunol* **12**, 624-630
27. Mehrotra, P., Krishnamurthy, P., Sun, J., Goenka, S., and Kaplan, M. H. (2015) Poly-ADP-ribosyl polymerase-14 promotes T helper 17 and follicular T helper development. *Immunology* **146**, 537-546
28. Mehrotra, P., Hollenbeck, A., Riley, J. P., Li, F., Patel, R. J., Akhtar, N., and Goenka, S. (2013) Poly (ADP-ribose) polymerase 14 and its enzyme activity regulates T(H)2 differentiation and allergic airway disease. *J Allergy Clin Immunol* **131**, 521-531 e521-512
29. Yan, Q., Dutt, S., Xu, R., Graves, K., Juszczynski, P., Manis, J. P., and Shipp, M. A. (2009) BBAP monoubiquitylates histone H4 at lysine 91 and selectively modulates the DNA damage response. *Mol Cell* **36**, 110-120
30. Hsiang, T. Y., Zhao, C., and Krug, R. M. (2009) Interferon-induced ISG15 conjugation inhibits influenza A virus gene expression and replication in human cells. *J Virol* **83**, 5971-5977
31. McNab, F., Mayer-Barber, K., Sher, A., Wack, A., and O'Garra, A. (2015) Type I interferons in infectious disease. *Nat Rev Immunol* **15**, 87-103
32. Jean Beltran, P. M., Mathias, R. A., and Cristea, I. M. (2016) A Portrait of the Human Organelle Proteome In Space and Time during Cytomegalovirus Infection. *Cell Syst* **3**, 361-373 e366

33. Jakobsen, L., Vanselow, K., Skogs, M., Toyoda, Y., Lundberg, E., Poser, I., . . . Andersen, J. S. (2011) Novel asymmetrically localizing components of human centrosomes identified by complementary proteomics methods. *EMBO J* **30**, 1520-1535
34. Law, A. H., Lee, D. C., Yuen, K. Y., Peiris, M., and Lau, A. S. (2010) Cellular response to influenza virus infection: a potential role for autophagy in CXCL10 and interferon-alpha induction. *Cell Mol Immunol* **7**, 263-270
35. Klionsky, D. J., Abdelmohsen, K., Abe, A., Abedin, M. J., Abeliovich, H., Acevedo Arozena, A., . . . Zughaier, S. M. (2016) Guidelines for the use and interpretation of assays for monitoring autophagy (3rd edition). *Autophagy* **12**, 1-222
36. Dengjel, J., Hoyer-Hansen, M., Nielsen, M. O., Eisenberg, T., Harder, L. M., Schandorff, S., . . . Andersen, J. S. (2012) Identification of autophagosome-associated proteins and regulators by quantitative proteomic analysis and genetic screens. *Mol Cell Proteomics* **11**, M111 014035
37. Nair, U., Thumm, M., Klionsky, D. J., and Krick, R. (2011) GFP-Atg8 protease protection as a tool to monitor autophagosome biogenesis. *Autophagy* **7**, 1546-1550
38. Matrosovich, M. N., Matrosovich, T. Y., Gray, T., Roberts, N. A., and Klenk, H. D. (2004) Human and avian influenza viruses target different cell types in cultures of human airway epithelium. *Proc Natl Acad Sci U S A* **101**, 4620-4624
39. Randall, R. E., and Goodbourn, S. (2008) Interferons and viruses: an interplay between induction, signalling, antiviral responses and virus countermeasures. *J Gen Virol* **89**, 1-47
40. Zhao, C., Hsiang, T. Y., Kuo, R. L., and Krug, R. M. (2010) ISG15 conjugation system targets the viral NS1 protein in influenza A virus-infected cells. *Proc Natl Acad Sci U S A* **107**, 2253-2258
41. Welsby, I., Hutin, D., and Leo, O. (2012) Complex roles of members of the ADP-ribosyl transferase super family in immune defences: looking beyond PARP1. *Biochem Pharmacol* **84**, 11-20
42. Juszczynski, P., Kutok, J. L., Li, C., Mitra, J., Aguiar, R. C., and Shipp, M. A. (2006) BAL1 and BBAP are regulated by a gamma interferon-responsive bidirectional promoter and are overexpressed in diffuse large B-cell lymphomas with a prominent inflammatory infiltrate. *Mol Cell Biol* **26**, 5348-5359
43. Emmott, E., Wise, H., Loucaides, E. M., Matthews, D. A., Digard, P., and Hiscox, J. A. (2010) Quantitative proteomics using SILAC coupled to LC-MS/MS reveals changes in the nucleolar proteome in influenza A virus-infected cells. *J Proteome Res* **9**, 5335-5345
44. Ohman, T., Rintahaka, J., Kalkkinen, N., Matikainen, S., and Nyman, T. A. (2009) Actin and RIG-I/MAVS signaling components translocate to mitochondria upon influenza A virus infection of human primary macrophages. *J Immunol* **182**, 5682-5692
45. Wu, X., Wang, S., Yu, Y., Zhang, J., Sun, Z., Yan, Y., and Zhou, J. (2013) Subcellular proteomic analysis of human host cells infected with H3N2 swine influenza virus. *Proteomics* **13**, 3309-3326
46. Kawaguchi, A., and Nagata, K. (2007) De novo replication of the influenza virus RNA genome is regulated by DNA replicative helicase, MCM. *EMBO J* **26**, 4566-4575
47. Gretzmeier, C., Eiselein, S., Johnson, G. R., Engelke, R., Nowag, H., Zarei, M., . . . Dengjel, J. (2017) Degradation of protein translation machinery by amino acid starvation-induced macroautophagy. *Autophagy* **13**, 1064-1075
48. Kraft, C., Deplazes, A., Sohrmann, M., and Peter, M. (2008) Mature ribosomes are selectively degraded upon starvation by an autophagy pathway requiring the Ubp3p/Bre5p ubiquitin protease. *Nat Cell Biol* **10**, 602-610
49. Liu, G., Zhong, M., Guo, C., Komatsu, M., Xu, J., Wang, Y., and Kitazato, K. (2016) Autophagy is involved in regulating influenza A virus RNA and protein synthesis associated with both modulation of Hsp90 induction and mTOR/p70S6K signaling pathway. *Int J Biochem Cell Biol* **72**, 100-108

50. Feizi, N., Mehrbod, P., Romani, B., Soleimanjahi, H., Bamdad, T., Feizi, A., . . . Abdoli, A. (2017) Autophagy induction regulates influenza virus replication in a time-dependent manner. *J Med Microbiol* **66**, 536-541

Figure Legends

Figure 1. IAV-induced changes of the host cell proteome. (A) SILAC labeled A549 cells were IAV infected for 24 h with a MOI of 2 or left untreated. Cells were either lysed (whole cell lysate (WCL)) or fractionated into cytosol, mitochondria, nuclei and vesicles. Lysates and fractions were mixed in a ratio of 1:1, respectively, and samples were prepared for MS analysis as outlined. All experiments were performed in two biological replicates with reversed labels. **(B)** Ratios of two biological replicates of WCL analyses were averaged and used to highlight IAV-regulated proteins. Grey dots represent unaffected proteins. Red dots represent proteins that significantly changed abundance upon IAV treatment (significance B, $p<0.05$, BH corrected). **(C)** STRING interaction network of significantly changed proteins in WCL and cellular compartments. Red marked proteins carry GO BP term “type I interferon signaling pathway”, yellow marked proteins carry KEGG term “Influenza A”. **(D)** A549 cells were either left untreated or infected with IAV for 24 h with a MOI of 2. Samples were analyzed by western blot with indicated antibodies. Actin served as loading control. **(E)** Immunofluorescence staining of untreated and IAV-treated A549 cells (MOI=4) for DTX3L and UBE2L6 (green), respectively, and DAPI (blue). Scale bars represent 10 µm.

Figure 2. IAV-induced changes of subcellular localizations of host proteins. (A) SILAC-work flow of cell fractionation analysis. SILAC-labeled A549 cells were IAV infected for 24 h (Arg10/Lys8) with a MOI of 2 or left untreated (Arg6/Lys4 and Arg0/Lys0). All labels were separated into nuclear, mitochondrial, cytosolic and vesicular fractions. The light labeled fractions were combined and the protein concentration of all fractions and all labels was determined. The separated fractions of untreated and infected cells were mixed in a 1:1 ratio and the same amount of the combined light fraction was spiked in as an internal standard. Samples were prepared for MS analysis as outlined. **(B)** Protein profiles of two biological replicates each were merged, standardized and clustered using the fuzzy c-means algorithm. Profiles separated into 8 clusters.

Color scale represents cluster membership values. **(C)** GO CC term enrichment analysis was used to detect enriched protein groups in respective clusters comparing IAV and untreated cells. Blue color represents unchanged enriched protein groups in the respective clusters, whereas changes are shown in red. **(D)** IAV-induced changes in the cellular localization of the MCM protein complex**.** Profiles of the 6 members of the MCM complex over the 4 compartments under the two different treatments are shown (standardized SILAC ratios). **(E)** Average nuclear SILAC ratios of MCM proteins compared to the internal standard are shown from untreated and infected cells resulting in a significant difference (*: $p<0.05$). Bars represent standard deviation. **(F)** Average nuclear intensity of MCM7 in untreated and infected cells as analyzed by IF analysis (***: $p<0.001$). **(G)** IAV-induced changes in the cellular localization of ribosomes. Gray lines represent the standardized SILAC profiles of all detected ribosomal proteins of the large ribosomal subunit (RPL). Black lines illustrate the average profiles. **(H)** Vesicular RPL4 intensity of untreated and infected cells as analyzed by western blot (n=3, **: $p<0.01$). Bars represent standard deviation.

Figure 3. IAV blocks functional autophagy. A549 GFP-LC3 cells were either left untreated, infected with IAV for 24 h (MOI = 2), treated for 7 h with 2 nM concanamycin A (conA), or infected for 24 h and treated for the last 7 h with 2 nM conA. **(A)** Immunofluorescence of untreated, conA treated and IAV infected A549 GFP-LC3 cells. The green dots represent autophagosomes, nuclear DAPI-staining is shown in blue. Scale bar represents 10 µm. **(B)** Immunoblot analysis of indicated host proteins of untreated, conA treated, IAV infected and IAV infected and conA treated A549 GFP-LC3 cells. GAPDH served as a loading control. **(C)** Level of autophagic flux of untreated and infected cells. The measured intensity of LC3-II was normalized to GAPDH and the relative autophagic flux was calculated by dividing LC3-II intensities of samples with conA by respective intensities without conA. Data of two biological replicates are shown relative to ctrl experiments.

Figure 4. IAV localizes to autophagosomes and changes the autophagosomal proteome. **(A)** PCP-SILAC workflow of isolation of autophagosomes via density gradient centrifugation. SILAC labeled cells were dounced and the vesicular fraction was applied on self-made iodixanol gradients for gradient centrifugation. Six fractions were collected and the light labeled fractions were mixed together and applied in a 1:1 ratio as an internal standard to the collected fractions of the heavy label. The combined samples were separated by SDS-PAGE, in-gel digested by trypsin, and analyzed by LC-MS/MS. **(B)** Western blot analysis of the autophagosomal marker protein LC3-II. Black bars indicate quantification. **(C)** Gradient profiles of viral and autophagosomal marker proteins**.** The gray lines represent the gradient distribution profile of all detected viral proteins. LC3 and GABARAPL indicate the distribution of autophagosomes over the gradient. **(D)** GO term enrichment of the autophagosomal clusters (AC) of conA and IAV treated cells. Content of AC of IAV and conA treated cells were analyzed with Perseus for enriched GO terms. A selection of enriched GO terms is shown and the number of proteins assigned to each particular GO term is shown in percent ($p<0.01$, BH corrected, minimum number of proteins in each category for enriched GO terms were 5).

Figure 5. IAV infections leads to localization of ribosomes and viral mRNA to autophagosomes. (A) Gradient profiles of ribosomal and autophagosomal marker proteins. The gray lines represent the gradient distribution profiles of all detected ribosomal proteins of the large subunit (RPL) of the corresponding treatment. LC3 and GABARAPL indicate the distribution of autophagosomes over the gradient. **(B)** Proteinase K protection assay. A549 GFP-LC3 cells were either stimulated with conA for 7 h or infected with IAV for 24 h. After differential centrifugation, the vesicular fraction was used for the protease protection assay. Shown are two biological replicates each. SQSTM1, RPL4 and LC3 were detected via western blot. **(C)** The RPL4 intensity was quantified relative to SQSTM1 and GFP-LC3-II (n=6). Error bars represent standard

deviations. **(D)** mRNA content of autophagosomes. mRNA was purified from the combined vesicular gradient fractions 2 and 3, 4 and 5, 6 and 7, respectively.

Figure 1

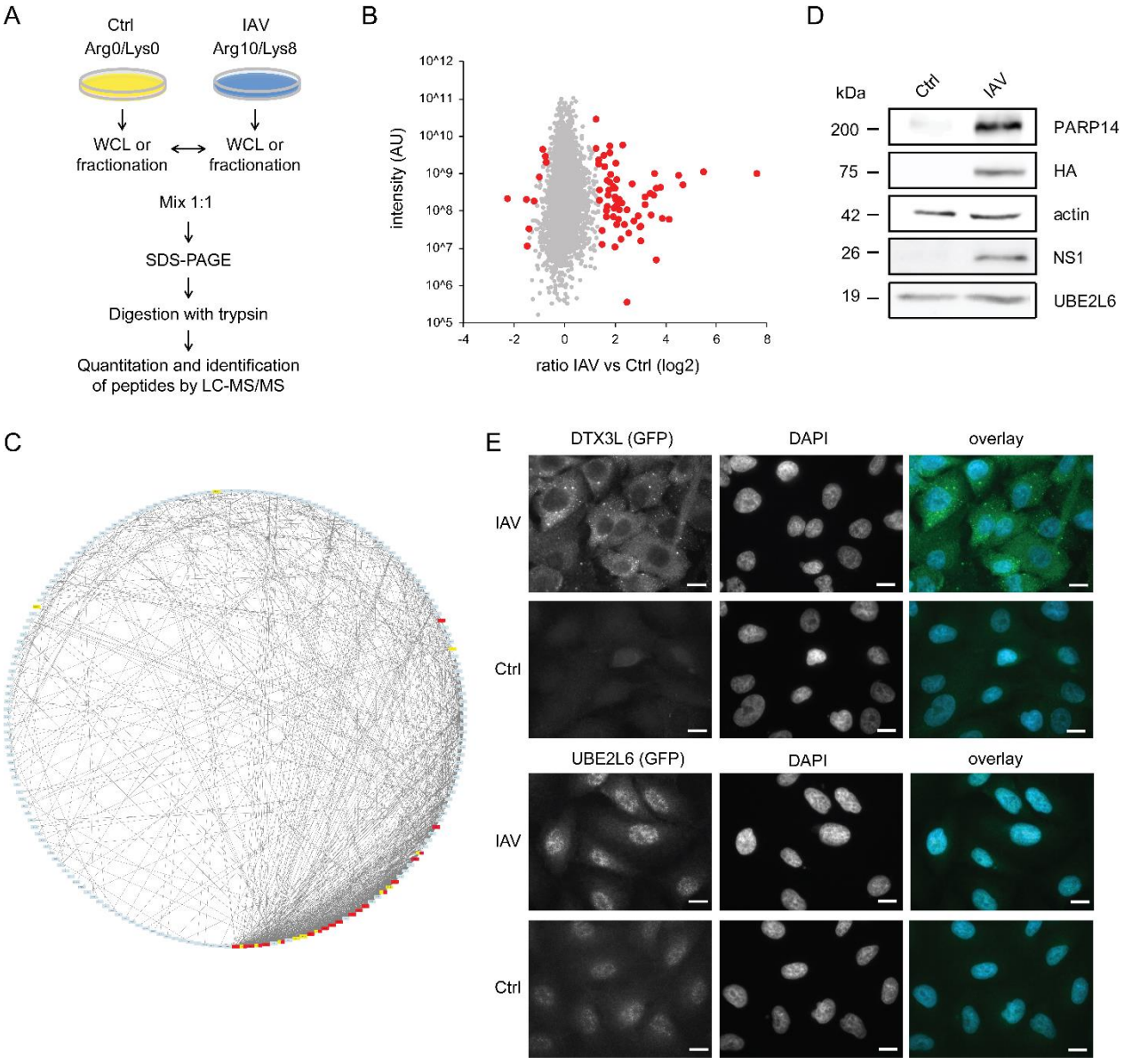
A
Ctrl
Arg0/Lys0
IAV
Arg10/Lys8
WCL or fractionation
WCL or fractionation
Mix 1:1
SDS-PAGE
Digestion with trypsin
Quantitation and identification of peptides by LC-MS/MS
B
intensity (AU)
ratio IAV vs Ctrl (log2)
D
kDa
Ctrl
IAV
200
75
42
26
19
PARP14
HA
actin
NS1
UBE2L6
C
E
DTX3L (GFP)
DAPI
overlay
IAV
Ctrl
UBE2L6 (GFP)
DAPI
overlay
IAV
Ctrl

Figure 2

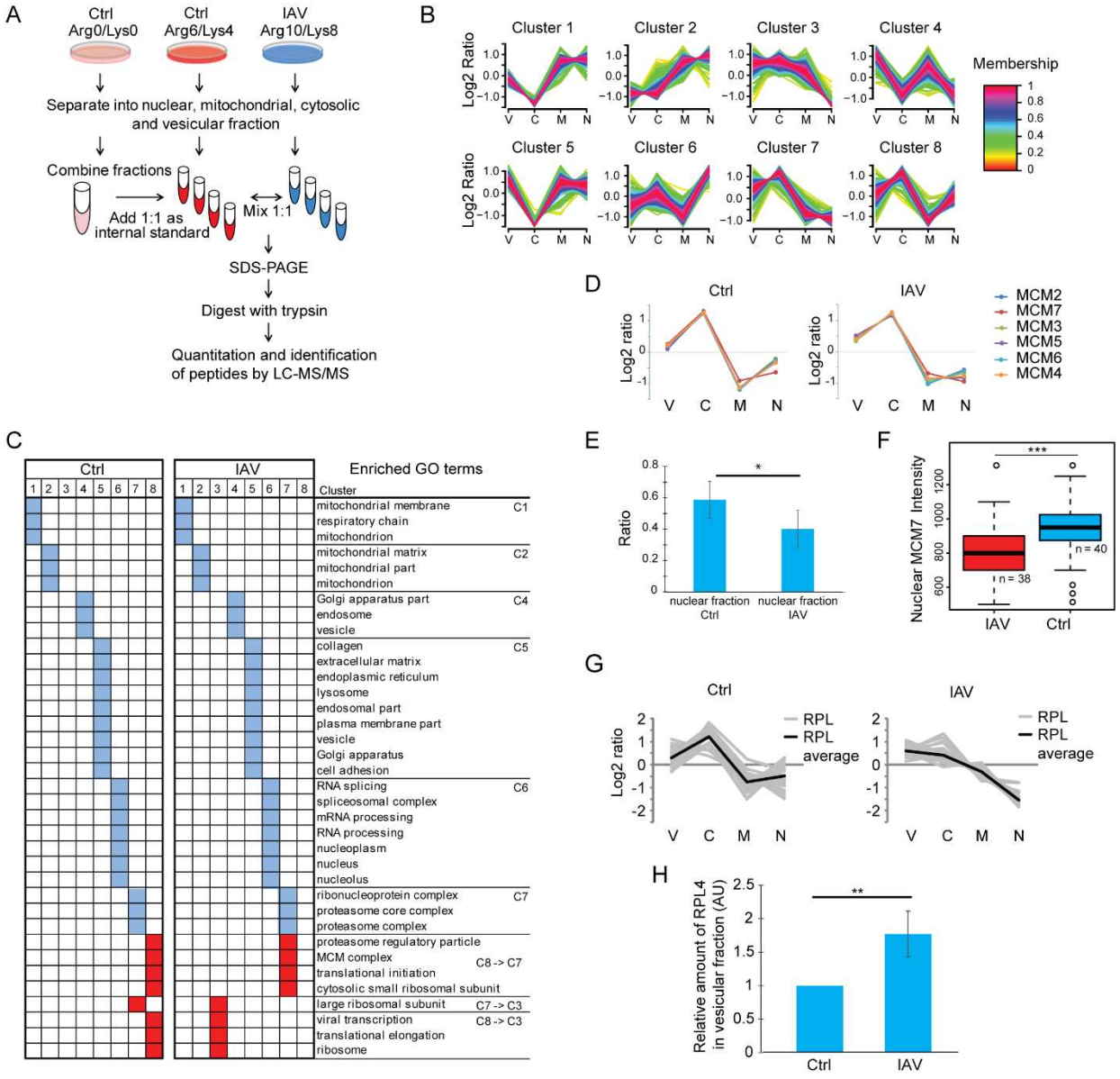
A
Ctrl Arg0/Lys0
Ctrl Arg6/Lys4
IAV Arg10/Lys8
Separate into nuclear, mitochondrial, cytosolic and vesicular fraction
Combine fractions
Add 1:1 as internal standard
Mix 1:1
SDS-PAGE
Digest with trypsin
Quantitation and identification of peptides by LC-MS/MS
B
Cluster 1
Cluster 2
Cluster 3
Cluster 4
Cluster 5
Cluster 6
Cluster 7
Cluster 8
Log2 Ratio
Membership
C
Ctrl
IAV
Enriched GO terms
Cluster
mitochondrial membrane
respiratory chain
mitochondrion
mitochondrial matrix
mitochondrial part
mitochondrion
Golgi apparatus part
endosome
vesicle
collagen
extracellular matrix
endoplasmic reticulum
lysosome
endosomal part
plasma membrane part
vesicle
Golgi apparatus
cell adhesion
RNA splicing
spliceosomal complex
mRNA processing
RNA processing
nucleoplasm
nucleus
nucleolus
ribonucleoprotein complex
proteasome core complex
proteasome complex
proteasome regulatory particle
MCM complex
translational initiation
cytosolic small ribosomal subunit
large ribosomal subunit
viral transcription
translational elongation
ribosome
C1
C2
C4
C5
C6
C7
C8 -> C7
C7 -> C3
C8 -> C3
D
Ctrl
IAV
Log2 ratio
MCM2
MCM7
MCM3
MCM5
MCM6
MCM4
E
Ratio
nuclear fraction Ctrl
nuclear fraction IAV
F
Nuclear MCM7 Intensity
n = 38
n = 40
IAV
Ctrl
G
Ctrl
IAV
Log2 ratio
RPL
RPL average
H
Relative amount of RPL4 in vesicular fraction (AU)
Ctrl
IAV

Figure 3

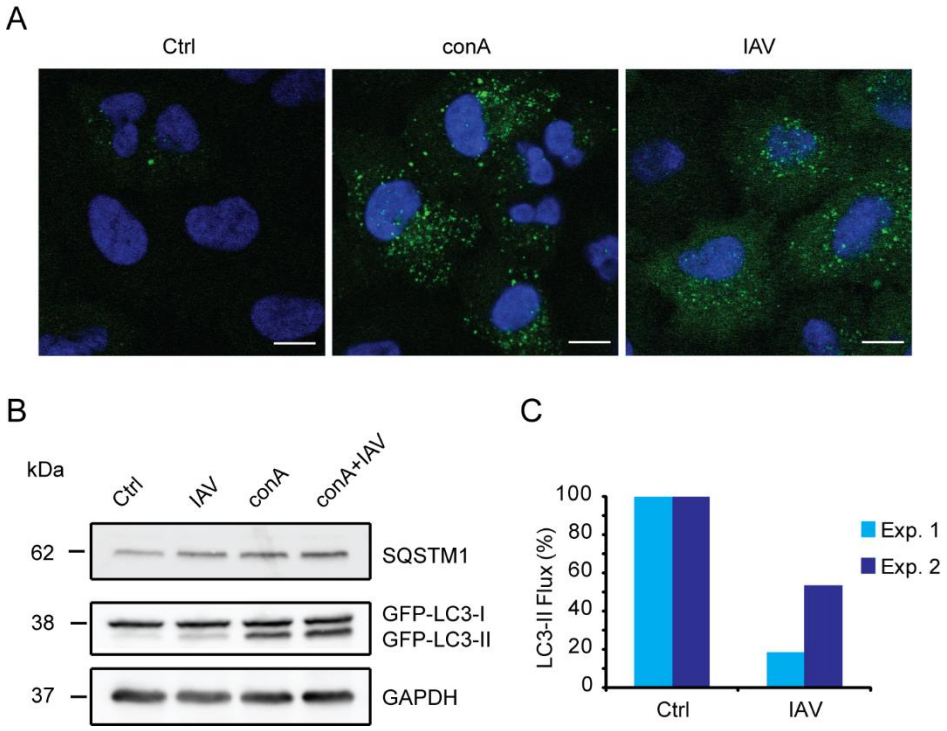
A
Ctrl
conA
IAV
B
kDa
Ctrl
IAV
conA
conA+IAV
62
SQSTM1
38
GFP-LC3-I
GFP-LC3-II
37
GAPDH
C
LC3-II Flux (%)
100
80
60
40
20
0
Ctrl
IAV
Exp. 1
Exp. 2

Figure 4

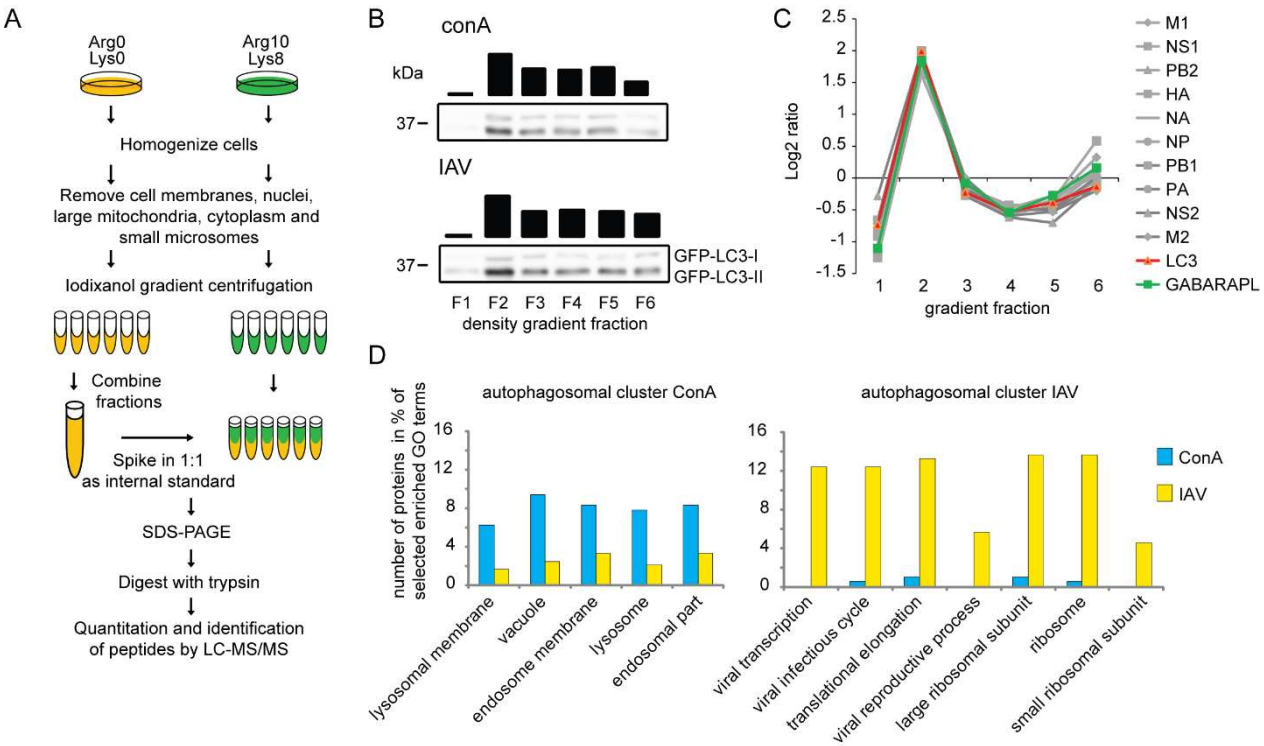
A
Arg0
Lys0
Arg10
Lys8
Homogenize cells
Remove cell membranes, nuclei, large mitochondria, cytoplasm and small microsomes
Iodixanol gradient centrifugation
Combine fractions
Spike in 1:1 as internal standard
SDS-PAGE
Digest with trypsin
Quantitation and identification of peptides by LC-MS/MS
B
conA
kDa
37–
IAV
37–
GFP-LC3-I
GFP-LC3-II
F1 F2 F3 F4 F5 F6
density gradient fraction
C
Log2 ratio
gradient fraction
M1
NS1
PB2
HA
NA
NP
PB1
PA
NS2
M2
LC3
GABARAPL
D
autophagosomal cluster ConA
autophagosomal cluster IAV
number of proteins in % of selected enriched GO terms
lysosomal membrane
vacuole
endosome membrane
lysosome
endosomal part
viral transcription
viral infectious cycle
translational elongation
viral reproductive process
large ribosomal subunit
ribosome
small ribosomal subunit
ConA
IAV

Figure 5

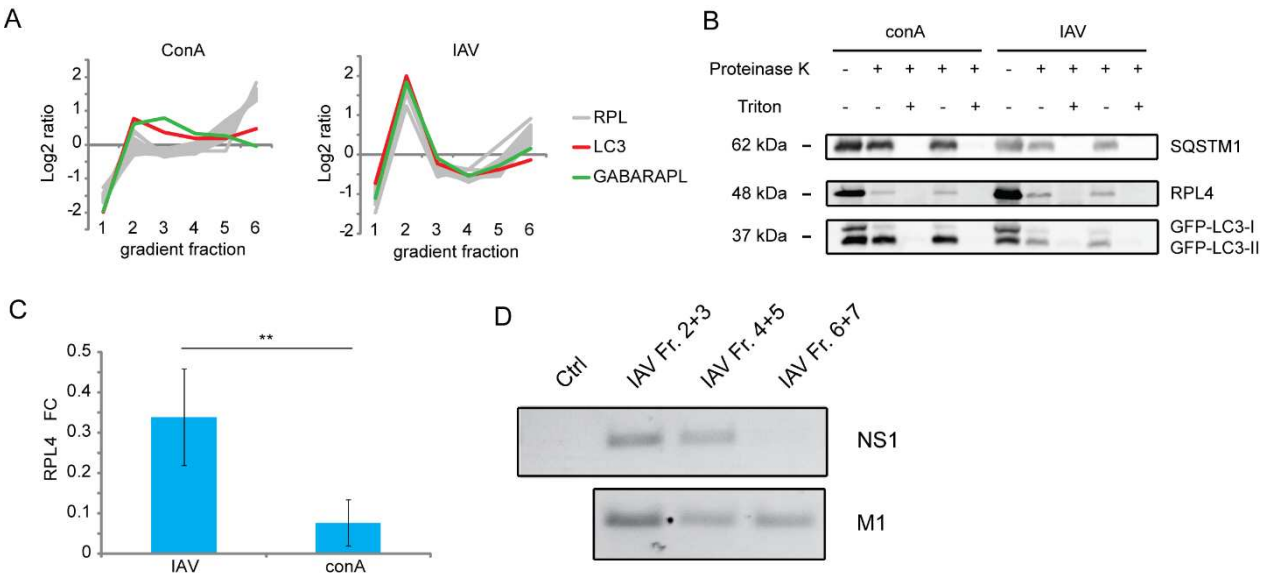
A
ConA
IAV
Log2 ratio
gradient fraction
RPL
LC3
GABARAPL
B
conA
IAV
Proteinase K
Triton
62 kDa
48 kDa
37 kDa
SQSTM1
RPL4
GFP-LC3-I
GFP-LC3-II
C
RPL4 FC
**
IAV
conA
D
Ctrl
IAV Fr. 2+3
IAV Fr. 4+5
IAV Fr. 6+7
NS1
M1